

Warping and precession in galactic and extragalactic accretion disksAnderson Caproni^{1,2}, Mario Livio², Zulema Abraham¹ and Herman J. Mosquera Cuesta^{3,4}**ABSTRACT**

The Bardeen-Petterson general relativistic effect has been suggested as the mechanism responsible for precession in some accretion disk systems. Here we examine separately four mechanisms (tidally-induced, irradiation-induced, magnetically-induced and Bardeen-Petterson-induced) that can lead to warping and precession. We use a sample of eight X-ray binaries and four Active Galactic Nuclei (AGNs) that present signatures of warping and/or precession in their accretion disks to explore the viability of the different mechanisms. For the X-ray binaries SMC X-1 and 4U 1907+09 all four mechanisms provide precession periods compatible with those observed, while for Cyg X-1 and the active galaxies Arp 102B and NGC 1068, only two mechanisms are in agreement with the observations. The irradiation-driven instability seems incapable of producing the inferred precession of the active galaxies in our sample, and the tidally-induced precession can probably be ruled out in the case of Arp 102B. Perhaps the best case for a Bardeen-Petterson precession can be achieved for NGC 1068. Our results show that given the many observational uncertainties that still exist, it is extremely difficult to confirm unambiguously that the Bardeen-Petterson effect has been observed in any of the other sources of our sample.

Subject headings: accretion, accretion disks — black hole physics — galaxies: active — galaxies: nuclei — magnetic fields — stars: neutron — X-rays: binaries

1. Introduction

The importance of accretion processes in the line formation and continuum emission in AGNs and galactic sources, such as microquasars and X-ray binaries, has long been recognized in the

¹Instituto de Astronomia, Geofísica e Ciências Atmosféricas, Universidade de São Paulo, R. do Matão 1226, Cidade Universitária, CEP 05508-900, São Paulo, SP, Brazil; acaproni@astro.iag.usp.br.

²Space Telescope Science Institute, 3700 San Martin Drive, Baltimore, MD, 21218.

³Instituto de Cosmologia, Relatividade e Astrofísica (ICRA-BR), Centro Brasileiro de Pesquisas Físicas, R. Dr. Xavier Sigaud 150, CEP 22290-180, Rio de Janeiro, RJ, Brazil; hermanjc@cbpf.br.

⁴Abdus Salam International Centre for Theoretical Physics, Strada Costiera 11, Miramare 34014, Trieste, Italy

literature, even though the presence of an accretion disk in some of those systems is inferred only indirectly.

The continuous improvement in the capability of telescopes and detectors to obtain high-resolution images, and spectra with higher sensitivity, allowed for the direct probing of the physical characteristics of some accretion disk systems (e.g., Ray et al. 1996; Jones et al. 2000; Jaffe et al. 2004; Fathi et al. 2006).

In contrast to the standard picture of a flat disk surrounding the accreting object, some galactic and extragalactic sources present signatures of warping and precession in their disks and/or jets (e.g., Margon 1984; Sillanpää et al. 1988; Abraham 2000; Gallimore et al. 2004; Caproni, Abraham & Mosquera Cuesta 2006). The apparent lack of correlation between the orientation of the radio jets and the plane of the host galaxy’s disk might also be attributed to warped disks (e.g., Schmitt et al. 2002).

The Bardeen-Petterson effect (Bardeen & Petterson 1975), a gravitational perturbation predicted by general relativity, is one of the physical mechanisms that has been proposed to explain warping and precession in accretion disks (e.g., Scheuer & Feiler 1996; Nelson & Papaloizou 2000; Fragile & Anninos 2005; King et al. 2005; Caproni, Abraham & Mosquera Cuesta 2006). In order to explore whether this mechanism is universal, in the sense that it can be acting in both galactic and extragalactic accretion disks, we have selected eight X-ray binaries and four AGNs that present signatures of warping/precession in their disks. We have analyzed individually the predictions of three additional precession mechanisms for the same sample of sources, in order to compare these predictions with those from the Bardeen-Petterson effect. In Section 2, we describe the accretion disk model used throughout the paper, as well as constraints on the basic parameters of the accretion disk. In Section 3, we present the four warping/precession mechanisms studied in this work. A brief introduction of the sample of sources, as well as their basic parameters (inferred observationally) is given in Section 4. A comparison between the theoretical predictions and observations is carried out in Section 5, and conclusions follow.

2. The accretion disk model

We consider an accretion disk through which mass is accreted onto a compact object (a black hole or a neutron star) at a mass accretion rate \dot{M} . The angular momentum of the accretion disk per unit area can be written as:

$$L_d(r) = \Sigma(r)\Omega(r)r^2, \tag{1}$$

where r is the radial distance from the compact object, Σ is the surface density of the accretion

disk (integrated over a scale height H), and Ω is the (relativistic) Keplerian angular velocity of the disk, given by (e.g., Abramowicz, Jaroszyński & Sikora 1978):

$$\Omega_{\text{K}}(r) = \frac{c}{R_{\text{g}}} \left[\left(\frac{r}{R_{\text{g}}} \right)^{3/2} + a_* \right]^{-1}, \quad (2)$$

where a_* is the ratio between the actual angular momentum of the compact object and its maximum possible value and $R_{\text{g}} = GM/c^2$ is the gravitational radius of the compact object, (where G and c are the gravitational constant and the speed of light respectively). Note that for $r \gg R_{\text{g}}$ or $a_* \simeq 0$, we recover the Newtonian angular velocity.

If the accretion disk is not self-gravitating, the scale height of the disk can be determined from hydrostatic equilibrium to be:

$$H(r) = \frac{c_{\text{s}}(r)}{\Omega(r)}, \quad (3)$$

where c_{s} is the sound speed, given by (e.g., Abramowicz et al. 1988):

$$c_{\text{s}}(r) = \sqrt{-\frac{5}{3} \frac{d \ln \Omega(r)}{d \ln r} \frac{\nu_1(r) \Omega(r)}{\alpha}}, \quad (4)$$

where α is the dimensionless viscosity parameter introduced by Shakura & Sunyaev (1973). The azimuthal kinematic viscosity of the disk, ν_1 , is calculated from (e.g., Krolik 1998):

$$\nu_1(r) = -\frac{\dot{M}}{2\pi\Sigma(r)} \left[\frac{d \ln \Omega(r)}{d \ln r} \right]^{-1} \left[1 - \left(\frac{R_{\text{ms}}}{r} \right)^2 \frac{\Omega(R_{\text{ms}})}{\Omega(r)} \right], \quad (5)$$

where R_{ms} is the radius of the innermost marginally stable orbit, assumed to be the inner radius of the disk¹.

In this work, we assume a power-law disk (e.g., Ostriker, Shu, & Adams 1992; Maloney, Begelman & Nowak 1998; Caproni, Abraham & Mosquera Cuesta 2004; Raymond, Quinn & Lunine 2005; Caproni, Abraham & Mosquera Cuesta 2006):

¹For neutron stars with strong magnetic fields, the accretion disk might be truncated at a larger radius than R_{ms} , at the magnetospheric radius. Even though this might be the case for some sources in our sample, it should not change our results in any substantial way.

$$\Sigma(r) = \Sigma_0 \left(\frac{r}{R_g} \right)^s, \quad (6)$$

where Σ_0 and s are constants.

For accretion disk models available in the literature, $-2 < s < 2$, while Σ_0 should be determined from some reasonable assumptions concerning each system.

An extreme upper limit for Σ_0 can be found by imposing that the accretion disk mass M_d is lower than the mass of the compact object, such that

$$\Sigma_0^{M_d} < \frac{c^2}{2\pi G} R_g^{s+1} \left(\int_{R_{\text{ms}}}^{R_{\text{out}}} r^{s+1} dr \right)^{-1}. \quad (7)$$

In order to estimate the limit on Σ_0 using equation (7), it is necessary to know the outer radius of the disk R_{out} , which is generally not well constrained by observations, especially for AGNs. For our AGN sample, we have adopted $R_{\text{out}} \sim 10^5 R_g$ based on the model of Collin-Souffrin & Dumont (1990), except for NGC 1068 in which interferometric maser observations indicate that its outer radius is at about 1.1 pc (Gallimore et al. 2004). In the case of binary systems in which accretion occurs via Roche lobe overflow, we take $R_{\text{out}} \approx 0.88 R_L$ (Papaloizou & Pringle 1977), where the Roche-lobe radius R_L is given by (Eggleton 1983):

$$R_L = \frac{0.49q^{2/3}}{0.6q^{2/3} + \ln(1 + q^{1/3})} R_{\text{ps}}, \quad (8)$$

where R_{ps} is the binary separation.

Another estimate for Σ_0 can be derived from the assumption that the accretion disk is self-gravitationally stable. This implies that the Toomre parameter $Q = c_s \Omega / (\pi G \Sigma)$ (Toomre 1964) must be greater than unity, which leads to:

$$\Sigma_0^Q < \left[\frac{5c^3}{6\pi^3 G^2 R_g^3} \frac{\dot{M}}{\alpha} \right]^{1/3} \left(\frac{R_{\text{out}}}{R_g} \right)^{-(s+3/2)} F_Q^{1/3}, \quad (9)$$

with the dimensionless function F_Q given by:

$$F_Q(a_*, R_{\text{out}}) = \left[\frac{1 - (R_{\text{ms}}/R_{\text{out}})^2 \Omega(R_{\text{ms}})/\Omega(R_{\text{out}})}{1 + a_* (R_{\text{out}}/R_g)^{-3/2}} \right]. \quad (10)$$

We can see that $F_Q \sim 1$ for $R_{\text{out}} \gg R_{\text{ms}}$, which is true for all the sources in our sample. The upper limit on Σ_0 corresponds to the minimum between $\Sigma_0^{M_d}$ and Σ_0^Q .

On the other hand, a lower limit for Σ_0 can be established from the requirement that the radial inflow is (highly) subsonic. This gives:

$$\Sigma_0^{v_r} > \frac{1}{\Upsilon^2} \frac{3\alpha\dot{M}}{10\pi c R_g} \left(\frac{R_{\text{out}}}{R_g}\right)^{-(s+1/2)} \left[1 + a_* \left(\frac{R_{\text{out}}}{R_g}\right)^{-3/2}\right]^{-1} F_Q. \quad (11)$$

where the Mach number $\Upsilon = v_r/c_s$, and v_r is radial velocity of the disk material. Although the requirement of a subsonic accretion inflow only implies that $\Upsilon < 1$, current accretion disk models usually give $\Upsilon \lesssim 0.01$ (e.g., Shakura & Sunyaev 1973; Abramowicz et al. 1988; Narayan & Yi 1995). Consequently, we have assumed $\Upsilon = 0.01$ in this work.

We therefore take for the allowed range of Σ_0 in this work: $\Sigma_0^{v_r} < \Sigma_0 < \min(\Sigma_0^{M_d}, \Sigma_0^Q)$. We should note that for the irradiation-driven instability, another lower limit on Σ_0 can be derived from considerations of the disk opacity (see § 3.2). However, in most of the cases analyzed in this work, $\Sigma_0^{v_r}$ has provided a more restrictive lower limit for Σ_0 .

3. Warp/Precession mechanisms

There are four main mechanisms that have been suggested for driving warping and precession in accretion disks. We consider all of these in turn.

3.1. Tidal forces of a companion object in a binary system

The precession of an accretion disk can be tidally induced by a companion in a binary system (e.g., Katz 1973; Sillanpää et al. 1988; Katz 1997; Romero et al. 2000; Caproni & Abraham 2004a).

We consider a binary system with masses M_p and M_s (for the primary and secondary, respectively), separated by a distance R_{ps} . From Kepler’s third law,

$$R_{\text{ps}}^3 = \frac{G(M_p + M_s)}{4\pi^2} P_{\text{orb}}^2, \quad (12)$$

where P_{orb} is the orbital period.

If the orbit is non-coplanar with the accretion disk, torques are induced in the inner parts of the disk, producing precession. Taking the outer radius of the precessing disk to be R_{prec} ($R_{\text{prec}} \leq R_{\text{out}}$;

Romero et al. 2000), the precession period, P_{prec} , is given by (Papaloizou & Terquem 1995; Larwood 1997):

$$P_{\text{prec}} \geq -\frac{8\pi}{3} \left(\frac{5-n}{7-2n} \right) \frac{R_{\text{ps}}^3}{R_{\text{prec}}^{3/2}} \frac{1}{\sqrt{GM_{\text{p}}q} \cos \theta}, \quad (13)$$

where n is the polytropic index of the gas (e.g., $n = 3/2$ for a non-relativistic gas and $n = 3$ for the relativistic case), $q = M_{\text{s}}/M_{\text{p}}$ and θ is the inclination angle of the orbit with respect to the disk plane. The negative sign in equation (13) indicates that the induced precession is retrograde, in the sense of being contrary to the rotation of the accretion disk.

Combining equations (12) and (13) (with the condition $R_{\text{prec}} \leq R_{\text{out}}$) we obtain:

$$P_{\text{prec}} \geq -\frac{4}{3} \left(\frac{5-n}{7-2n} \right) \left[\frac{(1+q)^{1/3}}{0.88q^{2/3}f(q)} \right]^{3/2} \frac{P_{\text{orb}}}{\cos \theta}, \quad (14)$$

where $f(q)$ is the function multiplying R_{ps} on the right-hand side of equation (8). Note that the ratio between the precession and orbital periods depends (apart from θ) primarily on the mass ratio of the binary system.

3.2. Radiation-driven instability

Radiation produced by the accreting compact object can modify the dynamics of an optically thick accretion disk. Petterson (1977) showed that if the disk is warped and optically thick, the radiation pressure will produce nonaxisymmetric torques that will change the initial warped configuration of the disk. Pringle (1996) and subsequently Maloney, Begelman & Pringle (1996) showed that even for an initially flat accretion disk, the radiation torques can warp and twist it. Pringle (1997) extended those calculations to include self-shadowing effects due to the warps. This radiation-driven instability has been invoked to explain anomalies in the morphology and variability in a huge variety of astrophysical sources (e.g., Cliffe et al. 1995; Maloney, Begelman & Pringle 1996; Southwell, Livio & Pringle 1997; Livio & Pringle 1997; Armitage & Pringle 1997; Wijers & Pringle 1999; Ogilvie & Dubus 2001).

Maloney, Begelman & Nowak (1998) generalized the isothermal disk model assumed in previous papers, and considered power-law surface density distributions ranging from the isothermal case ($s = -3/2$) to radiation-pressure dominated disks ($s = 3/2$). Solving numerically the twist differential equation governing such disks (without including self-shadowing), they found that the critical radius at which the disk becomes unstable is:

$$R_{\text{cr}} = x_{\text{cr}}^2 \left(\frac{\eta}{\epsilon}\right)^2 R_{\text{g}}, \quad (15)$$

where $\eta = \nu_2/\nu_1$ is the ratio between the vertical and the azimuthal viscosities in the disk, ϵ is the accretion efficiency and x_{cr} is equal to 2π for $s = -3/2$, increasing monotonically to $\sim 4.891\pi$ for $s = 3/2$.

In the steady-state regime, the precession period, $P_{\text{prec}}^{\text{rad}}$, due to the radiation-instability is (Maloney, Begelman & Nowak 1998):

$$P_{\text{prec}}^{\text{rad}} = \frac{4\pi^2}{\sigma_0} \tilde{\sigma}^{-1} \left(\frac{\eta}{\epsilon}\right)^{2s+3}, \quad (16)$$

where $8.74 \times 10^{-7} \leq \tilde{\sigma} \leq 1$ (lower and upper limits referring to $s = 3/2$ and $-3/2$ respectively), and the dimensionless parameter σ_0 is given by:

$$\sigma_0 = \frac{L_{\text{bol}}}{12c^2 \Sigma_0 R_{\text{g}}^2}, \quad (17)$$

where L_{bol} is the bolometric luminosity produced by the accretion process onto the compact object.

As we have noted in Section 2, the disk has to be optically thick in order to be unstable to warping by irradiation. This implies the existence of an independent lower limit for the surface density, represented by Σ_0^{r} , which is not necessarily more restrictive than Σ_0^{vr} .

Note also that Σ_0^{r} depends on which mechanism is the main contributor to the disk opacity; if Thomson scattering on free electrons of cross-section σ_{T} dominates over free-free absorption (with opacity κ_{ff}), the optical depth can be calculated from $\tau_{\text{T}} = \sqrt{\sigma_{\text{T}} \kappa_{\text{ff}} / m_{\text{H}}} \Sigma$, otherwise $\tau_{\text{ff}} = \kappa_{\text{ff}} \Sigma$ (Shakura & Sunyaev 1973).

The Rosseland mean opacity for free-free absorption is $\kappa_{\text{ff}} = \kappa_0 \rho T^{-7/2}$, where ρ and T are the mass density and temperature of the accretion disk respectively, while κ_0 is a numerical constant equal to $\sim 3 \times 10^{23} \text{ cm}^2 \text{ g}^{-1}$ (e.g., Maloney, Begelman & Nowak 1998). Expressing ρ and T in terms of Σ and c_{s} , and assuming a non-relativistic ideal equation-of-state for the gas in the disk, κ_{ff} is given as:

$$\kappa_{\text{ff}}(r) = \kappa_0 \left(\frac{5}{3} \frac{k_{\text{B}}}{\mu m_{\text{H}}}\right)^{7/2} \frac{\Sigma(r) \Omega(r)}{c_{\text{s}}^8(r)}, \quad (18)$$

where k_B is Boltzmann’s constant, μ is the mean molecular weight and m_H is the atomic Hydrogen mass.

If $\kappa_{\text{ff}} < \sigma_T/m_H$ at the critical radius, the lower limit on Σ_0 (in order to have an optically thick disk) is:

$$\Sigma_0^\tau > \left(\frac{m_H}{\sigma_T}\right)^{1/7} K_\tau^{1/7} \left(\frac{c}{R_g}\right)^{3/7} \left(\frac{\dot{M}}{\alpha}\right)^{4/7} \left(\frac{R_{\text{cr}}}{R_g}\right)^{-(s+9/14)} G_\tau, \quad (19)$$

where

$$K_\tau = \left(\frac{5}{6\pi}\right)^4 \left(\frac{5}{3} \frac{k_B}{\mu m_H}\right)^{-7/2} \kappa_0^{-1}, \quad (20)$$

and

$$G_\tau(a_*, R_{\text{cr}}) = \left[1 + a_* \left(\frac{R_{\text{cr}}}{R_g}\right)^{-3/2}\right]^{-1} F_Q^{-4/7}(a_*, R_{\text{cr}}). \quad (21)$$

On the other hand, if free-free absorption dominates:

$$\Sigma_0^\tau > K_\tau^{1/6} \left(\frac{c}{R_g}\right)^{1/2} \left(\frac{\dot{M}}{\alpha}\right)^{2/3} \left(\frac{R_{\text{cr}}}{R_g}\right)^{-(s+3/4)} G_\tau^{7/6}, \quad (22)$$

Thus, the lower limit for Σ_0 in the case of irradiation torques is obtained from the more restrictive value between $\Sigma_0^{\nu_r}$ (equation 11) and Σ_0^τ .

3.3. Magnetically-driven instability

The influence of magnetic fields on accretion disks has been studied by several authors, especially in the cases in which the central object is magnetized (e.g., Aly 1980; Lipunov & Shakura 1980; Lai 1999; Terquem & Papaloizou 2000). The production of quasi-periodic oscillations and luminosity variability in such objects has also been explored in the framework of external magnetic fields and accretion disk interactions (e.g., Agapitou, Papaloizou & Terquem 1997; Terquem & Papaloizou 2000; Shirakawa & Lai 2002a,b).

Lipunov & Shakura (1980) and Lai (1999) showed that when the spin axis of the magnetized object, as well as its dipole moment, are not aligned with the angular momentum of the disk, magnetic torques will be generated, causing warping and disk precession. Extending those results to non-magnetized central sources, Lai (2003) showed that a large-scale magnetic field (associated with magnetically driven outflows) threading the disk also induces a warping instability and a retrograde precession. Nonlinear simulations of warped, viscous accretion disks driven by magnetic torques were performed by Pfeiffer & Lai (2004). These numerical simulations showed that the disk can keep a steady-state warped shape with a rigid-body precession.

In order to examine the applicability of the magnetically driven mechanism to our sample of objects, we have considered a very idealized configuration, similar to that adopted by Lai (2003). Let us assume that the accretion disk is threaded by a poloidal magnetic field \vec{B}_p with a radial pitch angle $\varphi = \arctan |B_R/B_Z|$, where B_R and B_Z are respectively the radial and parallel magnetic field components in relation to the direction of the compact object’s rotation axis (Z-direction).

The poloidal magnetic field lines will be twisted by the disk rotation, generating a toroidal component B_Φ that has different signs above and below the disk plane due to the discontinuity of B_R at the disk mid-plane (Lai 2003). Following Lai (2003), we introduce the azimuthal pitch ζ , such that $B_\Phi = \mp\zeta B_Z$, with the negative and positive signs referring to B_Φ above and below the disk mid-plane, respectively.

In addition, the accretion disk plane does not have to be perpendicular to B_Z , being instead tilted by an angle β (see figure 2 in Lai 2003). In this case, the projection of B_Z onto the perpendicular direction (to the disk) will be $B_Z \cos \beta$, while the toroidal magnetic field will be $\mp\zeta B_Z \cos \beta$.

The discontinuities in the radial and toroidal components of the magnetic field inside the disk produce a net disk surface current. The interaction between the current’s toroidal component and the radial component of the magnetic field leads to the magnetically driven precession, while the interaction between the toroidal component of the magnetic field and the radial component of the net disk surface current warps the disk. The magnetic torques per unit area responsible for the disk precession and warping (averaged over the azimuthal angle ϕ) were calculated by Lai (2003):

$$\langle T_{\text{prec}}^{\text{mag}} \rangle_\phi = -\frac{\tan \varphi}{4\pi} r B_Z^2, \quad (23)$$

$$\langle T_{\text{warp}}^{\text{mag}} \rangle_\phi = -\frac{\zeta}{4\pi} r B_Z^2 \cos \beta. \quad (24)$$

We can see that this mechanism produces retrograde precession, as in the case of the tidal torques in binary systems, and it pulls the normal to the disk plane away from the B_Z -direction, increasing the angle β with time.

The precession period induced by the magnetic torques can be estimated by:

$$P_{\text{prec}}^{\text{mag}} = \frac{J_{\text{d}}(R_{\text{ms}}, R_{\text{prec}})}{\int_{R_{\text{ms}}}^{R_{\text{prec}}} \langle T_{\text{prec}}^{\text{mag}} \rangle_{\phi} r dr}, \quad (25)$$

where J_{d} is the integrated angular momentum of the accretion disk:

$$J_{\text{d}}(R_{\text{ms}}, R_{\text{prec}}) = 2\pi \int_{R_{\text{ms}}}^{R_{\text{prec}}} L_{\text{d}}(r) r dr. \quad (26)$$

The magnetic warping timescale can be calculated using:

$$P_{\text{warp}}^{\text{mag}} = \frac{J_{\text{d}}(R_{\text{ms}}, R_{\text{prec}})}{\int_{R_{\text{ms}}}^{R_{\text{prec}}} \langle T_{\text{warp}}^{\text{mag}} \rangle_{\phi} r dr}. \quad (27)$$

To calculate the precession timescale, we have assumed a power-law profile for B_{Z} , as in Lai (1998), such that:

$$B_{\text{Z}}(r) = B_{0,\text{Z}} \left(\frac{r}{R_{\text{g}}} \right)^{\chi}, \quad (28)$$

where $\chi = 0$ correspond to the case of a constant B_{Z} along the disk, while $\chi = -3$ corresponds to the dipole case.

Substituting our power-law parameterizations for Σ and B_{Z} into equation (25), we can calculate the relation between the observationally inferred precession period and Σ_0 and $B_{0,\text{Z}}$, expressed by the ratio $\tan \varphi P_{\text{prec}}^{\text{mag}} B_{0,\text{Z}}^2 / \Sigma_0$, as a function of the geometrical parameters a_* , R_{out} , s and χ .

3.4. Frame dragging and disk viscosity: the Bardeen-Petterson effect

Frame dragging produced by a rotating compact body with angular momentum J_{B} causes precession of a particle if its orbital plane is inclined in relation to the equatorial plane of the rotating object. This is known as the Lense-Thirring effect (Lense & Thirring 1918). The precession angular velocity Ω_{LT} produced by the frame dragging is given by (e.g., Wilkins 1972):

$$\Omega_{\text{LT}}(r) = \frac{2G}{c^2} \frac{J_{\text{B}}}{r^3}. \quad (29)$$

The presence of the Lense-Thirring effect in astrophysical systems with rotating neutron stars or Kerr black holes has been claimed in several works in the literature, as the physical mechanism behind the observed quasi-periodic oscillations (e.g., Cui, Zhang & Chen 1998; Stella & Vietri 1998; Markovic & Lamb 1998).

The combined action of the Lense-Thirring effect and the internal viscosity of the accretion disk forces the alignment between the angular momenta of the Kerr black hole and the accretion disk. This is known as the Bardeen-Petterson effect (Bardeen & Petterson 1975), and it tends to affect only the innermost part of the disk due to the short range of the Lense-Thirring effect, while the disk’s outer part tends to remain in its original configuration. The transition radius between these two regimes is known as the Bardeen-Petterson radius, R_{BP} , and its location depends mainly on the physical properties of the accretion disk (Bardeen & Petterson 1975; Kumar & Pringle 1985; Ivanov & Illarianov 1997; Nelson & Papaloizou 2000).

A rough estimate of R_{BP} can be obtained by comparing the time-scales for Lense-Thirring precession and warp transmission through the disk (e.g., Natarajan & Armitage 1999). If the transmission occurs diffusively, the Bardeen-Petterson radius can be obtained from:

$$R_{\text{BP}}^{\text{diff}} = \sqrt{\frac{\nu_2(r = R_{\text{BP}}^{\text{diff}})}{\Omega_{\text{LT}}(r = R_{\text{BP}}^{\text{diff}})}}. \quad (30)$$

The diffusive regime in a Bardeen-Petterson disk has been explored by several authors (e.g., Kumar & Pringle 1985; Scheuer & Feiler 1996; Nelson & Papaloizou 2000; Fragile & Anninos 2005; Lodato & Pringle 2006), either using analytical calculations or numerical methods.

A Bardeen-Petterson disk in a wave-like regime has also been studied in the literature (e.g., Ivanov & Illarianov 1997; Ogilvie 1999; Lubow, Ogilvie & Pringle 2002); in such a situation, R_{BP} is given by:

$$R_{\text{BP}}^{\text{w}} = \frac{c_s(r = R_{\text{BP}}^{\text{w}})}{\Omega_{\text{LT}}(r = R_{\text{BP}}^{\text{w}})}. \quad (31)$$

The transition between the diffusive and wave-like regimes occurs approximately at a radius $R_{\text{T}} \sim H/\alpha$ (Papaloizou & Lin 1995).

The time-scale for the black hole to align its angular momentum with that of the accretion disk was first estimated by Rees (1978). Scheuer & Feiler (1996) obtained an analytic solution to the equations that control the warp evolution in the case of a disk with constant surface density and used that to calculate the alignment time-scale. Natarajan & Armitage (1999) generalized the results found by Scheuer & Feiler (1996) to a power-law viscosity. These studies suggest that the alignment time-scale can be estimated by:

$$T_{\text{align}} = J_{\text{B}} \left(\frac{dJ_{\text{B}}}{dt} \right)^{-1} \sin \varphi, \quad (32)$$

where φ is the angle between the angular momentum of the neutron star/black hole J_{B} and the direction perpendicular to the outer disk, and the time derivative of J_{B} is given by:

$$\frac{dJ_{\text{B}}}{dt} = -2\pi \sin \varphi \int_{R_{\text{BP}}}^{R_{\text{out}}} \Omega_{\text{LT}}(r) L_{\text{d}}(r) r dr. \quad (33)$$

Contrary to Scheuer & Feiler (1996), King et al. (2005) showed that counter-alignment can occur when the spins are anti-parallel ($\varphi > \pi/2$) and the angular momentum on the disk is smaller than about twice that of the rotating compact object ($J_{\text{d}} < 2J_{\text{B}}$). The results obtained recently by Lodato & Pringle (2006) support the possible existence of counter-alignment.

Other than in the special circumstances mentioned above, the Bardeen-Petterson effect forces the disk to align gradually with the rotating compact object. According to Scheuer & Feiler (1996), the time evolution of the alignment, and the precession period of the disk angular momentum around the spin axis of the rotating accreting object, $P_{\text{prec}}^{\text{BP}}$, are given by:

$$\varphi(t) = \varphi_0 e^{-\Delta t/T_{\text{align}}} \quad (34)$$

$$P_{\text{prec}}^{\text{BP}}(t) = P_0 e^{-\Delta t/T_{\text{align}}} \quad (35)$$

where $\Delta t = t - t_0$, and φ_0 and P_0 are, respectively, the inclination angle and precession period at time t_0 , when the action of the Bardeen-Petterson torques over the accretion disk started ($t_0 \leq 0$ is measured in the past from the present time). Scheuer & Feiler (1996) found that the timescales for precession and realignment are identical, implying that $P_0 = T_{\text{align}}$, which will also be used here.

4. Source sample

To analyze separately the consequences of each of the precession mechanisms discussed in the last section, we selected eight X-ray binaries and four AGNs that present signatures of warping and/or precession in their accretion disks. In this section we introduce these systems and provide their basic parameters (the ones that will be used in our calculations).

X-ray binaries, characterized as semi-detached systems with one component filling its critical Roche lobe, can be roughly divided into two categories: high- and low-mass X-ray binaries (HMXBs and LMXBs respectively).

HMXBs are composed of an accreting compact source (a black hole or a neutron star) and either an OB supergiant or a Be star (van Paradijs 1983), which implies that such systems are short-lived, with ages of less than about 2×10^7 yr (van den Heuvel 1994). They are spatially distributed in the galactic plane, being associated with young stellar populations.

By contrast, LMXBs contain a neutron star accreting from a low-mass star ($\lesssim 2M_{\odot}$). They are typically associated with an older stellar population, with ages of about one Gyr (van den Heuvel 1994).

Here, we will use eight X-ray binaries with regular (or quasi-regular) precession periods inferred basically from the optical and X-ray continuum variability, as well as from variability in the line intensity and velocity in some cases. Our sample is composed of two LMXBs (Her X-1 and Cyg X-2) and six HMXBs, four of which have an accreting neutron star (LMC X-4, Cen X-3, SMC X-1 and 4U 1907+09) while the remaining sources are black hole systems (SS 433 and Cyg X-1). It is important to note that SS 433 is one of the best studied microquasars in the literature, with a prominent precessing jet/counterjet (e.g., Hjellming & Johnston 1981; Margon 1984; Blundell et al. 2001; Blundell & Bowler 2004). The relevant parameters of the sources, for the present work, are listed in Table 1. In particular, the values of the magnetic field strength listed in Table 1 refer basically to the surface magnetic fields of neutron stars, while for the two black hole systems we used values derived from dynamo models for the disk magnetic field (Pudritz & Fahlman 1982; Rose 1995).

Some AGNs also exhibit signatures of warping/precession in their accretion disks. The signatures are in the form variability of double-peaked Balmer lines and of the continuum emission, or distortions in the jet morphology (variations in the jet orientation and jet velocity) (e.g., Abraham 2000; Storchi-Bergmann et al. 2003; Caproni & Abraham 2004b). We have selected four AGNs with these characteristics: the Seyfert 1 galaxy 3C 120, the Seyfert 2 galaxy NGC 1068, the broad-line radio galaxy Arp 102B, and the BL Lac OJ 287. Their parameters are listed in Table 2. In relation to their magnetic field strengths, since there is evidence in some cases that the strength of the magnetic field is not in equipartition (e.g. Coker & Melia 2000), we have chosen the field strength to be equal to that which has been observationally determined in a few AGN ($\sim 10^4$ G; e.g., Field & Rogers 1993; Lobanov 1998).

5. Analysis

We have analyzed which of the four mechanisms can be driving the observed precession in the twelve sources of our sample. Below we describe the results of this analysis, discussing each mechanism separately.

5.1. Tidal torques in a binary system

In order to examine the possibility that tidal torques induced by the companion affect the accretion disk, we have plotted in the left panel of Figure 1 the quantity $\cos\theta P_{\text{prec}}/P_{\text{orb}}$ predicted by equation (14) as a function of q (thick line); the values for all the X-ray binaries in our sample are also displayed (star symbols). The values of θ for Her X-1, LMC X-4, SS 433 and Cyg X-1 were taken from the literature (Heemskerk & van Paradijs 1989; Scott et al. 2000; Stirling et al. 2002; Romero et al. 2002), while $\theta = 10^\circ$ was assumed for the other X-ray binaries.

The gray regions in Figure 1 show the part of parameter space where tidal torques from a companion can drive precession. Clearly, the observed ratios between the precession and orbital periods for Cen X-3 and Cyg X-2 reside below of this region. Therefore, the origin of their disk precession cannot be attributed to the tidal torques of the secondary. In the case of Cyg X-1, Lachowicz et al. (2006) have recently claimed that its observed precession is prograde, which would also rule out the tidal torque scenario. For the other five X-ray binaries, precession may be induced by the torques of the companion star. Although Katz (1973) and Larwood (1998) have already proposed that tidal torques could lead to the observed precession in a few of these sources, tidally-induced precession has not been previously suggested (to the best of our knowledge) for 4U 1907+09.

In the case of the AGN sources, there is no straightforward observation that supports the existence of a supermassive binary black hole system in any of their nuclear regions. Nevertheless, the continuum variability and the anomalous jet kinematics in OJ 287 and 3C 120 have been used to put some constraints on the physical parameters of a possible binary system (Sillanpää et al. 1988; Abraham 2000; Caproni & Abraham 2004b). In the right-hand panel of Figure 1, we show the upper limit for $\cos\theta P_{\text{prec}}/P_{\text{orb}}$ as a function of q for our extragalactic sources, considering a timescale for losses due to gravitational radiation τ_{GW} (Shapiro & Teukolsky 1983) of 1000 yr. Although this value has been chosen arbitrarily, it guarantees that no significant changes in the orbit of the secondary occur on such a timescale, so that the observed precession periods do not vary substantially. Note that increasing (decreasing) τ_{GW} by a factor of 10 results in a decrease (increase) in the upper limit for $\cos\theta P_{\text{prec}}/P_{\text{orb}}$ only by a factor of ~ 2.4 . For OJ 287, 3C 120 and NGC 1068, θ was taken from the literature (Abraham 2000; Caproni & Abraham 2004b; Caproni, Abraham & Mosquera Cuesta 2006), while for Arp 102B, we assumed $\theta = 10^\circ$.

By contrast with the galactic binaries, we do not expect $q \gtrsim 1$ in supermassive binary black hole systems, since the expectation is generally that the accretion disk responsible for the AGN activity is associated with the more massive black hole. Except for Arp 102B, it is always possible to find a value of $q \leq 1$ for which $\cos\theta P_{\text{prec}}/P_{\text{orb}}$ is within the gray area. In addition, the separations between the putative black holes in NGC 1068 obtained from our calculations² are always smaller than the dimensions of the maser disk. Consequently, we would expect a more complex disk morphology than that suggested by the observations. Thus, tidal forces of an orbiting black hole

²Typically $100\text{-}10^4 R_g$, depending on the timescales for losses due to gravitational radiation.

can (in principle at least) induce the inferred precession rate in 3C 120 and OJ 287 (and perhaps NGC 1068).

5.2. Irradiation-driven torques

In Figures 2 and 3 we present the precession period induced by the radiation torques as a function of the critical radius at which the disk becomes irradiation-warping unstable, for each source of our sample, using equations (15) and (16). Following Maloney, Begelman & Nowak (1998), the calculations were performed for power-law disks, using $s = -3/2, -1, 0$ and $3/2$. The lower and upper limits for each solution refer to the respective lower and upper limits of Σ_0 calculated from equations (9), (11) and (19), as discussed previously.

The critical radius, as well as the precession period, depend on the ratio between η and ϵ , which is usually unknown. We have assumed $0.0377 \leq \epsilon \leq 0.42$ ³, while $1 \leq \eta \leq f(\alpha)$, where $f(\alpha) = 2(1 + 7\alpha^2)/[\alpha^2(4 + \alpha^2)]$ (Ogilvie 1999). In the case of $\eta = 1$ (open symbols in Figures 2 and 3), $2.38 \leq \eta/\epsilon \leq 26.49$, implying $223.80 \leq R_{\text{cr}}/R_{\text{g}} \leq 2.77 \times 10^4$ for $s = -3/2$ and $1.34 \times 10^3 \leq R_{\text{cr}}/R_{\text{g}} \leq 1.66 \times 10^5$ for $s = 3/2$. For $\eta \neq 1$, η/ϵ , and consequently $P_{\text{prec}}^{\text{rad}}$ and R_{cr} , also depend on the value of α ; we have chosen $\alpha = 0.1$ for the X-ray binaries and $\alpha = 0.01$ for the AGNs, except for NGC 1068 for which $0.001 \lesssim \alpha \lesssim 0.012$ (Caproni, Abraham & Mosquera Cuesta 2006). These values of α imply that the critical radii, for a fixed ϵ , are systematically larger in the case of $\eta \neq 1$.

For the X-ray binaries, in the case of an isothermal disk ($s = -3/2$) with $\eta = 1$ (open circles), the predicted precession period intervals cross the horizontal line, which represents the observed precession period. This indicates that the radiation instability can be responsible for precession in those X-ray binaries (for this particular accretion disk model). However, the situation changes when we take into account other combinations among s , η and ϵ ; even though the predictions assuming $s = -3/2$ and $\eta \neq 1$ are compatible with the observed precession in most cases, power-law disks with $s = 3/2$ generally fail to reproduce the observations, providing incompatible precession periods and/or critical radii larger than the outer disk radii.

As pointed out by Maloney, Begelman & Nowak (1998), disk precession induced by radiation must be prograde in the absence of external torques, which would be in contradiction with the observations of SS 433, Her X-1 and LMC X-4. However, as shown by Maloney & Begelman (1997) and corroborated by Maloney, Begelman & Nowak (1998), the quadrupole torque from a companion star might allow for the existence of prograde and retrograde precession modes. Thus, retrograde precession due to the irradiation mechanism is possible only if there is some additional torque acting upon the accretion disk.

³The upper and lower limits correspond to the accretion efficiencies from the maximum prograde and retrograde spinning black holes, respectively.

In the case of AGNs, the situation is quite different. For $\eta \neq 1$, the critical radius is larger than the outer disk radius for all AGNs in our sample, suggesting that in these cases the disk is stable against radiation torques.

Thus, the irradiation instability can be responsible for the precession in our sample of X-ray binaries, in agreement with Ogilvie & Dubus (2001), but it is not favored in the case of the AGNs we have considered.

5.3. Magnetically-driven torques

To analyze the precession induced by magnetic torques, we created a two-dimensional grid of the quantity $\tan \varphi P_{\text{prec}}^{\text{mag}} B_{0,Z}^2 / \Sigma_0$, fixing s and χ , as a function of a_* and R_{out} for each source in our sample.

These grids are plotted in Figures (4) and (5) for the X-ray binaries and in Figure (6) for the AGNs assuming power-law disks with $s = -2, -1$ and 0 and power-law magnetic field configurations with $\chi = 0, -1, -2$ and -3 . The gray area represents the allowed range for $P_{\text{prec}}^{\text{mag}} B_{0,Z}^2 / \Sigma_0$ (assuming $\tan \varphi = 1$) using the available constraints obtained from the observations. As in the case of tidal torques in binary systems, acceptable solutions must also obey $R_{\text{prec}} \leq R_{\text{out}}$. The dimensionless spin parameter influences only the location of the inner radius of the accretion disk, while the estimated extreme values for Σ_0 are responsible for the limits of the gray region in the panels of the Figures (4)-(6).

We can see in Figures (4)-(6) that not all magnetic field configurations provide solutions compatible with the observations. Nevertheless, it is possible to find combinations of s and χ that reproduce the observed precession periods, which means that magnetically-driven instabilities cannot be excluded as a potential mechanism for the observed precession.

At least in the case of the X-ray binaries with an accreting neutron star, such as Her X-1, LMC X-4, Cen X-3, Cyg X-2, SMC X-1 and 4U 1907+09, the magnetic field configuration is dipolar to a good approximation (e.g., Aly 1980). We have not found any possibility that disk precession in those systems can be associated with magnetic field configurations with $\chi \geq -1$, except for Cyg X-2 for which acceptable solutions are obtained with $\chi = -1$ and $\chi = 0$ only if $s = -2$. For the black hole X-ray binaries, Cyg X-1 has similar results to those of Cyg X-2, while for the microquasar SS 433 lower values of χ are strongly favored.

In contrast to the neutron star X-ray binaries, there is no preferred magnetic field configuration in the case of AGNs. Our results show that the range of the allowed solutions is systematically narrower than that obtained for the X-ray binaries. In addition, it seems to have two different regimes in our AGN sample: if the accretion disk surface density decreases faster with radial distance, with $s \lesssim -1$, the z-component of the magnetic field must be radially constant in order to reproduce the observed precession periods; otherwise, it is necessary for the surface density not to

vary radially ($s = 0$) if the magnetic field decreases along the disk ($\chi \leq -1$).

5.4. Bardeen-Petterson effect

In order to study the consequences of the Bardeen-Petterson effect in our sample of sources, we have separated the black hole systems from those with accreting neutron stars. In the former case, we have calculated the Bardeen-Petterson radius and the alignment timescale for six values of the black hole spin ($a_* = \pm 0.1, \pm 0.5$ and ± 1) and for $s = -2, -1$ and 0 , as shown in Figure 7. As in the previous sections, calculations were performed for $\eta = f(\alpha)$ ($\alpha = 0.1$ and 0.01 for X-ray binaries and AGNs, respectively) and $\eta = 1$, as well as for the estimated lower and upper limits on the accretion disk surface density.

Once s and η are fixed, there are generally two values of R_{BP} that are determined by the lower and upper limits of Σ_0 . In some cases the lower limit for Σ_0 leads to $R_{\text{BP}} < R_{\text{ms}}$, and because of that only the upper limit is shown in the figure. All sources have their Bardeen-Petterson radius inside of the outer edge of the disk, independently of the specific values for s , η and Σ_0 , which indicates that the Bardeen-Petterson mechanism is at least applicable.

We also plot in Figure 7 the time interval necessary for each system to reach the observationally inferred precession period (using equation 35). As in the case of the alignment timescales, the plots were truncated at 13.7 Gyr, the age of the Universe as inferred from the WMAP results (Bennett et al. 2003). Unfortunately, only in the case of SS 433 we can constrain better the allowed model parameters using its estimated age (between 2×10^4 and 2×10^5 yr; Zealey, Dopita, & Malin (1980)). This age constraint clearly favors model disks with $\eta \neq 1$ at least for $|a_*| \leq 0.1$. The same conclusions are valid for Cyg X-1 if we take into account the upper limit for the age of HMXBs (van den Heuvel 1994).

In the case of NGC 1068, we also have included the solutions obtained from a power-law accretion disk with $s = -1.05$ (Huré 2002), corresponding to model A shown in Figure 2 of Caproni, Abraham & Mosquera Cuesta (2006). Indeed, these authors showed that the Bardeen-Petterson effect can reproduce the disk configuration suggested by the maser observations (Gallimore et al. 2004), as well as the general shape of the parsec and kiloparsec radio jet.

For the neutron star systems in our sample, the spin period of the accreting neutron stars, P_s , are known, and are listed in Table 3. From the definition of the angular momentum parameter, we can obtain (e.g., Stella & Vietri 1998):

$$a_* = \frac{2\pi c}{G} \frac{I_p}{M_p} \frac{\nu_s}{M_p} \quad (36)$$

where I_p and ν_s are respectively the moment of inertia and the spin frequency of the neutron star.

If we write $I_p = 10^{45} I_{45} \text{ g cm}^2$ and $M_p = M_o M_\odot$ typically, $0.5 < I_{45}/M_o < 2$, considering rotating neutron star models for different equations of state and masses. In Table 3 we give the allowed ranges of a_* for our neutron star systems using their respective orbital periods and the lower and upper limits for I_{45}/M_o .

In Figure 8, we plot the results for the neutron star system displaying, as in the Figure 7, the Bardeen-Petterson radius, the alignment timescale and the time interval necessary for each system reach the observationally inferred precession period for the maximum absolute value of a_* listed in Table 3. As in the case of the Kerr black holes, all sources have their respective Bardeen-Petterson radii inside the outer radius of the accretion disk. All spinning neutron stars in our sample reach the observed precession periods in a timescale shorter than 20 Myr. In the case of Her X-1, whose age has been estimated previously (Verbunt, Wijers & Burm 1990), any allowed combination of model parameters leads to Her X-1 reaching its observed precession period via the Bardeen-Petterson effect. The situation is similar, even though somewhat more restrictive, for Cyg X-2.

6. Conclusions

In this work, we have selected eight X-ray binaries and four AGNs that present signatures of precession in their accretion disks in order to examine the compatibility between their precession periods and the predictions from four distinct warping/precession physical mechanisms: tidal torques from a companion in a binary system, irradiation- and magnetically-driven instabilities, and the Bardeen-Petterson relativistic effect.

We have assumed a power-law surface density distribution for the accretion disks, constraining their physical parameters from observational data available in the literature.

For the X-ray binaries in our sample, we found that tidal torques from a companion in a binary system provide precession timescales compatible with those inferred in SS 433, Her X-1, LMC X-4 and SMC X-1, as indeed has been previously suggested in the literature (Katz 1973; Larwood 1998). In addition, we showed that tidal torques can also drive precession in 4U 1907+09, which (as far as we know) had not been proposed before this work. The mechanism can be ruled out for Cen X-3 and Cyg X-2. In the case of our AGN sample (assuming that they contain binary black holes), we have shown that tidal torques cannot produce the disk precession inferred in Arp 102B.

Although the irradiation-driven instability usually provides precession timescales that agree with those observed in our X-ray binary sample, it is unsuccessful in reproducing the reported precession periods for the four AGNs considered here. The critical radii at which those AGN accretion disks become unstable against radiation torques were found to be larger than the expected disks' outer radii (for $\eta \neq 1$). Since the irradiation-driven instability produces prograde disk precession, the retrograde precession observed in SS 433, Her X-1 and LMC X-4 may only be generated in the presence of some external torques.

We have shown that torques due to a misaligned magnetic field (with respect to the perpendicular direction to an accretion disk) can also reproduce the observed precession periods of our sample. For the accreting neutron stars, a dipolar configuration must be a good approximation to their magnetic fields; in such a case (or for $\chi < -1$), the magnetic-driven torquing can induce precession in the inner parts of the accretion disks at the rate inferred observationally. For the black hole X-ray binaries, magnetic configurations with $\chi \geq -1$ are favored. Although the geometry of the magnetic field is not usually constrained by observations in AGNs, our results indicate the existence of two distinct regimes: for accretion disks with $s \lesssim -1$, the z-component of the magnetic field must be radially constant in order to reproduce the observed precession periods; otherwise, it is necessary to have a constant surface density ($s = 0$) with a magnetic field weakening radially along the disk ($\chi \leq -1$). In addition, if the accretion disk of Cyg X-1 is actually precessing progradely (Lachowicz et al. 2006), we can rule out magnetically-driven torques as the cause of its precession.

The Bardeen-Petterson effect produces precession timescales compatible with those observed in all sources of our sample, considering that the alignment of the accretion disk evolves on a similar timescale (as in Scheuer & Feiler 1996). The timescale for reaching the observed precession rate is usually shorter than the estimated lifetime of the sources. Considering the accretion disk parameters used in this work, we have found that all sources in our sample have Bardeen-Petterson radii smaller than the disk’s outer radius.

NGC 1068, for which maser observations have been used to infer the physical properties of the accretion disk, may provide the strongest candidate for the Bardeen-Petterson effect. In this case, we have shown that the irradiation-driven instability is incompatible with the observations. Tidal torques are also highly unlikely (even if a binary black hole were to be present in this system) since it would most likely result in other changes to the disk morphology, which are not observed. Magnetically-driven torques would work only if a rather contrived field configuration exists (B_z constant along the precessing part of the disk). Our conclusions give further support to the analysis of Caproni, Abraham & Mosquera Cuesta (2006), who showed that the Bardeen-Petterson effect is consistent with the warping morphology suggested by Gallimore et al. (2004).

The Bardeen-Petterson precession is an important general-relativistic effect, and its unambiguous detection would be of great value. This work has shown, however, that given the many observational uncertainties that still exist (both in X-ray binaries and in AGNs), it is extremely difficult to rule out definitively other precession mechanisms.

It is important to emphasize that although we have analyzed separately the four precession mechanisms in this work, they are not mutually exclusive. This means that more than one mechanism might be operating in a given system.

A.C. acknowledges financial support from FAPESP (Procs. 03/13882-0 and 05/56266-2), as well as the hospitality of the Space Telescope Science Institute, where this work was carried out.

REFERENCES

- Abraham, Z. 2000, *A&A*, 355, 915.
- Abramowicz, M., Jaroszyński, M., Sikora, M. 1978, *A&A*, 63, 221
- Abramowicz, M. A., Czerny, B., Lasota, J. P., Szuszkiewicz, E. 1988, *ApJ*, 332, 646
- Agapitou, V., Papaloizou, J. C. B., Terquem, C. 1997, *MNRAS*, 292, 631
- Altschuler, D. R. 1989, *Fundam. Cosmic Phys.*, 14, 37
- Aly, J. J. 1980, *A&A*, 86, 192
- Armitage, P. J., Pringle, J. E. 1997, *ApJ*, 488, L47
- Ash, T. D. C., Reynolds, A. P., Roche, P., Norton, A. J., Still, M. D., Morales-Rueda, L. 1999, *MNRAS*, 307, 357
- Bardeen, J. M., Petterson, J. A. 1975, *ApJ*, 195, L65
- Baykal, A., Inam, Ç., Ali Alpar, M., in't Zand, J. Strohmayer, T. 2001, *MNRAS*, 327, 1269
- Bennett, C. L., Halpern, M., Hinshaw, G., et al. 2003, *ApJS*, 148, 1.
- Blundell, K. M., Mioduszewski, A. J., Muxlow, T. W. B., Podsiadlowski, P., Rupen, M. P. 2001, *ApJ*, 562, L79
- Blundell, K. M., Bowler, M. G. 2004, *ApJ*, 616, L159
- Brinkmann, W., Kawai, N., Matsuoka, M. 1989, *A&A*, 218, L13
- Brockopp, C., Fender, R. P., Larionov, V., et al. 1999, *MNRAS*, 309, 1063
- Burderi, L., Di Salvo, T., Robba, N. R., La Barbera, A., Guainazzi, M. 2000, *ApJ*, 530, 429
- Campana, S. 2000, *ApJ*, 534, 79
- Caproni, A., Abraham, Z. 2004a, *MNRAS*, 349, 1218
- Caproni, A., Abraham, Z. 2004b, *ApJ*, 602, 625
- Caproni, A., Abraham, Z. & Mosquera Cuesta, H. J. 2004, *ApJ*, 616, L99
- Caproni, A., Abraham, Z. & Mosquera Cuesta, H. J. 2006, *ApJ*, 638, 120
- Casares, J., Charles, P., Kuulkers, E. 1998, *ApJ*, 493, L39
- Cliffe, J. A., Frank, A., Livio, M., Jones, T. W. 1995, *ApJ*, 447, 49

- Coburn, W., Heindl, W. A., Rothschild, R. E., et al. 2002, *ApJ*, 580, 394
- Coker, R. F., Melia, F. 2000, *ApJ*, 534, 723
- Collin-Souffrin, S., Dumont, A. M. 1990, *A&A*, 229, 292
- Cui, W., Zhang, S. N., Chen, W. 1998, *ApJ*, 492, L53
- dal Fiume, D., Orlandini, M., Cusumano, G. et al. 1998, *A&A*, 329, 41
- Eggleton, P. P. 1983, *MNRAS*, 204, 449
- Fathi, K., Storchi-Bergmann, T., Riffel, R. A., Winge, C., Axon, D. J., Robinson, A., Capetti, A., Marconi, A. 2006, *astro-ph/0602002*
- Field, G. B., Rogers, R. D. 1993, *ApJ*, 403, 94
- Focke, W. B. 1996, *ApJ*, 470, L127
- Fragile, P. C., Anninos, P. 2005, *ApJ*, 623, 347
- Gallimore, J. F., Baum, S. A., & O’Dea, C. P. 2004, *ApJ*, 613, 794
- Gerend, D., Boynton, P. E. 1976, *ApJ*, 209, 56
- Giacconi, R., Gursky, H., Kellogg, E., Levinson, R., Schreier, E., Tananbaum, H. 1973, *ApJ*, 184, 227
- Gies, D. R., Huang, W. & McSwain, M. V., 2002, *ApJ*, 578, L67
- Heemskerk M. H. M., van Paradijs J., 1989, *A&A*, 223, 154
- Herrero, A., Kudritzki, R. P., Gabler, R., Vilchez, J. M., Gabler, A. 1995, *A&A*, 297, 556
- Hjellming, R. M., Johnston, K. J. 1981, *Nature*, 290, 100
- Huré, J.-M. 2002, *A&A*, 395, L21
- int Zand, J. J. M., Baykal, A., Strohmayer, T. E. 1998, *ApJ*, 496, 386
- Ivanov, P. B., Illarianov, A. F. 1997, *MNRAS*, 285, 394.
- Jaffe, W., et al. 2004, *Nature*, 429, 47
- Jones, D. L., Wehrle, A. E., Meier, D. L., Piner, B. G. 2000, *ApJ*, 534, 165
- Kahabka, P., Li, X.-D. 1999, *A&A*, 345, 117
- Katz, J. I. 1973, *Nature Phys. Sci.*, 246, 87

- Katz, J. I. 1997, *ApJ*, 478, 527
- King A. R., Lubow S. H., Ogilvie G. I., Pringle J. E. 2005, *MNRAS*, 363, 49
- Kolb, U., Davies, M. B., King, A., Ritter, H. 2000, *MNRAS*, 317, 438
- Krolik, J. H. 1998, *Active Galactic Nuclei: From the Central Black Hole to the Galactic Environment* (Princeton: Princeton Univ. Press)
- Kumar, S., Pringle, J. E. 1985, *MNRAS*, 213, 435.
- La Barbera, A., Burderi, L., Di Salvo, T., Iaria, R., Robba, N. R. 2001, *ApJ*, 553, 375
- Lachowicz, P., Zdziarski, A. A., Schwarzenberg-Czerny, A., Pooley, G. G., Kitamoto, S. 2006, *astro-ph/0508306*
- Lai, D. 1998, *ApJ*, 502, 721
- Lai, D. 1999, *ApJ*, 524, 1030
- Lai, D. 2003, *ApJ*, 591, L119
- Lanzafame, G., Belvedere, G. 1998, *MNRAS*, 295, 618
- Larwood, J. D. 1997, *MNRAS*, 290, 490
- Larwood, J. D. 1998, *MNRAS*, 299, L32
- Leibowitz, E. M. 1984, *MNRAS*, 210, 279
- Lense, J., Thirring, H. 1918, *Phys. Z.*, 19, 156.
- Levine, A., Rappaport, S., Putney, A., Corbet, R., Nagase, F. 1991, *ApJ*, 381, 101
- Lipunov, V. M., Shakura, N. I. 1980, *Soviet Astron. Lett.*, 6, 14
- Livio, M., Pringle, J. E. 1997, *ApJ*, 486, 835
- Lobanov, A. P. 1998, *A&A*, 330, 79
- Lodato, G., Pringle, J. E. 2006, *astro-ph0602306*
- Lubow, S. H., Ogilvie, G. I. & Pringle, J. E. 2002, *MNRAS*, 337, 706
- Maloney, P. R., Begelman, M. C., Pringle, J. E. 1996, *ApJ*, 472, 582
- Maloney, P. R., Begelman, 1997, *ApJ*, 491, L43
- Maloney, P. R., Begelman, M. C., Nowak, M. A. 1998, *ApJ*, 504, 77

- Margon, B. 1984, *ARA&A*, 22, 507
- Markovic, D., Lamb, F. K. 1998, *ApJ*, 507, 316
- Mukerjee, K., Agrawal, P. C., Paul, B., Rao, A. R., Yadav, J. S., Seetha, S., Kasturirangan, K. 2001, *ApJ*, 548, 368
- Narayan, R., Yi, I. 1995, *ApJ*, 452, 710
- Natarajan, P., Armitage, P. J. 1999, *ApJ*, 506, L97
- Nelson, R. P., Papaloizou, J. C. B. 2000, *MNRAS*, 315, 570
- Netzer, H. 1990, in *Active Galactic Nuclei*, ed. R. D. Blandford, H. Netzer & L. Woltjer (Berlin: Springer), 57
- Newman, J. A., Eracleous, M., Filippenko, A. V., Halpern, J. P. 1997, *ApJ*, 485, 570
- Ogilvie, G. I. 1999, *MNRAS*, 304, 557
- Ogilvie, G. I., Dubus, G. 2001, *MNRAS*, 320, 485
- Okuda, T. 2002, *PASJ*, 54, 253
- Oosterbroek, T., Parmar, A. N., Sidoli, L., in't Zand, J. J. M., Heise, J. 2001, *A&A*, 375, 922
- Orosz, J. A., Kuulkers, E. 1999, *MNRAS*, 305, 132
- Ostriker, E. C., Shu, F. H., Adams, F. C. 1992, *ApJ*, 399, 192
- Papaloizou, J. C. B., Lin, D. N. C. 1995, *ApJ*, 438, 841
- Papaloizou, J. C. B., Pringle, J. E. 1977, *MNRAS*, 181, 441
- Papaloizou, J. C. B., Terquem, C. 1995, *MNRAS*, 274, 987
- Paul, B., Raichur, H., Mukherjee, U. 2005, *A&A*, 442, L15
- Peterson, B. M.; Ferrarese, L.; Gilbert, K. M., et al. 2004, *ApJ*, 613, 682
- Petterson, J. A. 1977, *ApJ*, 216, 827
- Pfeiffer, H. P., Lai, D. 2004, *ApJ*, 604, 766
- Priedhorsky, W. C., Terrell, J. 1983, *ApJ*, 273, 709
- Priedhorsky, W. C., Terrell, J. 1984, *ApJ*, 280, 661
- Priedhorsky, W. C., Brandt, S., Lund, N. 1995, *A&A*, 300, 415

- Pringle, J. E. 1996, MNRAS, 281, 357
- Pringle, J. E. 1997, MNRAS, 292, 136
- Pudritz, R. E., Fahlman, G. G. 1982, MNRAS, 198, 689
- Ray, T. P., Mundt, R., Dyson, J. E., Falle, S. A. E. G., Raga, A. C., 1996, ApJ, 468, L103
- Raymond, S. N., Quinn, T., Lunine, J. I. 2005, ApJ, 632, 670
- Rees, M. J. 1978, Nature, 275, 516
- Reynolds, A. P., Hilditch, R. W., Bell, S. A., Hill, G. 1993, MNRAS, 261, 337
- Reynolds, A. P., Quaintrell, H., Still, M. D., Roche, P., Chakrabarty, D., Levine, S. E. 1997, MNRAS, 288, 43
- Rose, W. K. 1995, MNRAS, 276, 1191
- Romero, G. E., Chajet, L., Abraham, Z., Fan, J. H. 2000, A&A, 360, 57
- Romero, G. E., Kaufman Bernadó, M. M., Mirabel, I. F. 2002, A&A, 393, L61
- Scheuer P. A. G., Feiler R. 1996, MNRAS, 282, 291
- Schmitt H. R., Pringle J. E., Clarke C. J., Kinney A. L., 2002, ApJ, 575, 150
- Schreier, E., Giacconi, R., Gursky, H., Kellogg, E., Tananbaum, H. 1972, ApJ, 178, L71
- Scott, D. M., Leahy, D. A., Wilson, R. B. 2000, ApJ, 539, 392
- Shakura, N. I., Sunyaev, R. A. 1973, A&A, 24, 337
- Shapiro, S. L., Teukolsky, S. A. 1983, in Black Holes, White Dwarfs and Neutron Stars, John Wiley & Sons, New York
- Shirakawa, A., Lai, D. 2002a, ApJ, 564, 361
- Shirakawa, A., Lai, D. 2002b, ApJ, 565, 1134
- Sillanpää, A., Haarala, S., Valtonen, M. J., Sundelius, B., Byrd, G. G. 1988, ApJ, 325, 628
- Southwell, K. A., Livio, M., Pringle, J. E. 1997, ApJ, 478, L29
- Stella, L., Vietri, M. 1998, ApJ, 492, L59
- Stewart, G. C., Watson, M. G., Matsuoka, M., et al. 1987, MNRAS, 228, 293
- Stirling, A. M., Jowett, F. H., Spencer, R. E., Paragi, Z., Ogley, R. N., Cawthorne, T. V. 2002, MNRAS, 337, 657

- Storchi-Bergmann, T., et al. 2003, *ApJ*, 598, 956
- Tananbaum, H., Gursky, H., Kellogg, E. M., Levinson, R., Schreier, E., Giacconi, R. 1972, *ApJ*, 174, L143
- Terquem, C., Papaloizou, J. C. B. 2000, *A&A*, 360, 1031
- Toomre, A. 1964, *ApJ*, 139, 1217
- Tsygankov, S. S., Lutovinov, A. A. 2005, *Astronomy Letters*, 31, 380
- van den Heuvel, E. P. J. 1994, in *Interacting Binaries*, ed. H. Nussbaumer & A. Orr (Berlin:Springer Verlag), 263
- van der Klis, M., Bonnet-Bidaud, J. M., Robba, N. R. 1980, *A&A*, 88, 8
- van Paradijs, J. 1983, in *Accretion Driven Stellar X-ray Sources*, ed. W. H. G. Lewin & E. P. J. van den Heuvel, (New York: Cambridge University Press), 189
- Verbunt, F., Wijers, R. A. M. J., Burm, H. M. G. 1990, *A&A*, 234, 195
- Vrtilek, S. D., Raymond, J. C., Garcia, M. R., Verbunt, F., Hasinger, G., Kurster, M. 1990, *A&A*, 235, 162
- Vrtilek, S. D., Boroson, B., Cheng, F. H., McCray, R., Nagase, F. 1997, *ApJ*, 490, 377
- Wang, J.-M., Luo, B., Ho, L. C. 2004, *ApJ*, 615, L9
- Wijers, R. A. M. J., Pringle, J. E. 1999, *MNRAS*, 308, 207
- Wijnands, R. A. D., Kuulkers, E., Smale, A. P. 1996, *ApJ*, 473, 45
- Wilkins, D. C. 1972, *Phys. Rev. D*, 5, 814
- Wilson, A. S., & Ulvestad, J. S. 1987, *ApJ*, 319, 105
- Wojdowski, P., Clark, G. W., Levine, A. M., Woo, J. W.; Zhang, S. N. 1998, *ApJ*, 502, 253
- Wojdowski, P. S., Clark, G. W., Kallman, T. R. 2000, *ApJ*, 541, 963
- Woo, J.-H., Urry, C. M. 2002, *ApJ*, 579, 530
- Wu, X.-B., Liu, F. K. 2004, *ApJ*, 614, 91
- Zealey, W. J., Dopita, M. A., Malin, D. F. 1980, *MNRAS*, 192, 731
- Zdziarski, A. A., Poutanen, J., Paciesas, W. S., Wen, L. 2002, *ApJ*, 578, 357

Table 1. Physical parameters of the X-ray binary sources.

Source	M_p (M_\odot)	Ref.	q^b	P_{orb} (d)	Ref.	P_{prec} (d)	Ref.	Type ^d	Ref.	B (G)	Ref.	L_{bol} (erg s^{-1}) ^f	Ref.
SS 433	11 ± 3	1	1.73	13.08	8	162.5	15	R	23,24	10^5	28	39.74	36
Her X-1	1.50 ± 0.30	2	1.53	1.7	9	34.88	16	R	25	3.5×10^{12}	29	37.58	2
LMC X-4	1.38 ± 0.25	3	10.6	1.408	3	30.275	17	R	26	10^{13}	30	38.19	37
Cen X-3	1.21 ± 0.21	4	16.9	2.087	10	140 ^c	18	?	-	3.5×10^{12}	31	37.88	38
Cyg X-1	10.1	5	1.76	5.67	11	142	19	P	27	10^{8e}	32	37.80	39
Cyg X-2	1.78 ± 0.23	6	0.34	9.844	12	77.7	20	?	-	4.5×10^{8c}	33	37.65	40
SMC X-1	1.60 ± 0.10	7	10.75	3.893	13	60	21	?	-	7.6×10^{12}	34	38.30	41
4U 1907+09	1.4 ^a	-	21.4	8.375	14	41.6	22	?	-	2.1×10^{12}	35	37.72 ^g	42

References. — (1) Gies, Huang & McSwain 2002; (2) Reynolds et al. 1997; (3) Levine et al. 1991; (4) Ash et al. 1999; (5) Herrero et al. 1995; (6) Orosz & Kuulkers 1999; (7) Reynolds et al. 1993; (8) Stewart et al. 1987; (9) Tananbaum et al. 1972; (10) Paul, Raichur & Mukherjee 2005; (11) Priedhorsky, Brandt & Lund 1995; (12) Casares, Charles & Kuulkers 1998; (13) Schreier et al. 1972; (14) in't Zand et al. 1998; (15) Stirling et al. 2002; (16) Giacconi et al. 1973; (17) Tsygankov & Lutovinov 2005; (18) Priedhorsky & Terrell 1983; (19) Brocksopp et al. 1999; (20) Wijnands, Kuulkers & Smale 1996; (21) Wojdowski et al. 1998; (22) Priedhorsky & Terrell 1984; (23) Leibowitz 1984; (24) Brinkmann, Kawai & Matsuoka 1989; (25) Gerend & Boynton 1976; (26) Heemskerck & van Paradijs 1989; (27) Lachowicz et al. 2006; (28) Rose 1995; (29) dal Fiume et al. 1998; (30) La Barbera et al. 2001; (31) Burderi et al. 2000; (32) Pudritz & Fahlman 1982; (33) Campana 2000; (34) Kahabka & Li 1999; (35) Coburn et al. 2002; (36) Okuda 2002; (37) Vrtilik et al. 1997; (38) Lanzafame & Belvedere 1998; (39) Zdziarski et al. 2002; (40) Vrtilik et al. 1990; (41) Wojdowski, Clark & Kallman 2000; (42) Mukerjee et al. 2001.

^aMass value assumed in this work;

^bQuoted errors obtained from error propagation;

^cMean value;

^dType of precession (in relation to the angular momentum of the accretion disk: prograde (P), retrograde (R). The symbol "?" indicates that there is no available information;

^eUpper limit;

^fBase-10 logarithm of the bolometric luminosity;

^gFlare state (upper limit).

Table 2. Physical parameters of the AGNs.

Source	M_{tot} ($10^8 M_{\odot}$)	Ref.	P_{prec} (yr) ^a	Ref.	Type ^c	B (G) ^d	L_{bol} (erg s^{-1}) ^e	Ref.
NGC 1068	0.120	1	$(2.08\text{-}35.2)\times 10^{3\text{b}}$	5	?	10^4	44.84^{f}	9
3C 120	0.556	2	11.9	6	?	10^4	45.34	10
OJ 287	6.170	3	8.88	7	?	10^4	44.44^{g}	3
Arp 102B	1.380	4	2.15	8	?	10^4	43.41	4

References. — (1) Huré 2002; (2) Peterson et al. 2004; (3) Wang, Luo & Ho 2004; (4) Wu & Liu 2004; (5) Caproni, Abraham & Mosquera Cuesta 2006; (6) Caproni & Abraham 2004b; (7) Abraham 2000; (8) Newman et al. 1997; (9) Gallimore et al. 2004; (10) Woo & Urry 2002.

^aValues measured at the present time and in the source’s reference frame;

^bObtained from the jet kinematics and the Bardeen-Petterson model (Caproni, Abraham & Mosquera Cuesta 2006);

^cSame nomenclature of the Table 1;

^dAdopted value for the magnetic field at R_g ;

^eBase-10 logarithm of the bolometric luminosity;

^fThis value is a lower limit;

^gAssuming also that the bolometric luminosity is about ten times larger than the luminosity of the broad line region (Netzer 1990).

Table 3. Rotation period and spin parameter for the neutron stars in our X-ray binaries sample.

Source	P_s (s)	Ref.	a_* ^a
Her X-1	1.2377697 ± 0.0000003	1	$(1.92\text{-}7.69)\times 10^{-4}$
LMC X-4	13.509 ± 0.002	2	$(1.91\text{-}7.66)\times 10^{-5}$
Cen X-3	4.834477 ± 0.000007	3	$(0.61\text{-}2.44)\times 10^{-4}$
Cyg X-2	0.00606 ± 0.00024	4	$(0.33\text{-}1.32)\times 10^{-1}$
SMC X-1	0.706707 ± 0.000001	5	$(0.32\text{-}1.26)\times 10^{-3}$
4U 1907+09	440.5738 ± 0.0002	6	$(0.58\text{-}2.31)\times 10^{-6}$

References. — (1) Oosterbroek et al. 2001; (2) Vrtilik et al. 1997; (3) van der Klis, Bonnet-Bidaud & Robba 1980; (4) Focke 1996; (5) Kahabka & Li 1999; (6) Baykal et al. 2001.

^aThe lower and upper limits refer respectively to $I_{45}/M_o = 0.5$ and 2 (Stella & Vietri 1998).

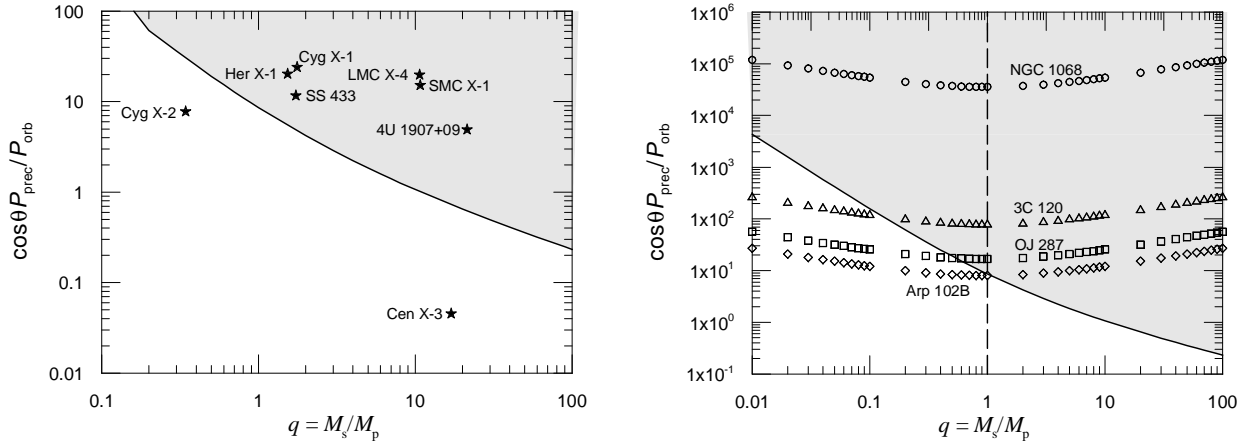


Fig. 1.— Precession due to tidal torques induced by the companion in binary systems. *Left panel:* Ratio between the precession and orbital periods (multiplied by the cosine of the inclination angle of the orbital plane in relation to the disk plane) as a function of the mass ratio between the secondary and primary objects. The solid line is the theoretical prediction considering that the entire disk with an outer radius of $0.88R_L$ precesses rigidly. Data from our sample of X-ray binaries are displayed by the stars. Sources located in the gray area can have their disk precession driven by the companion’s torque. *Right panel:* Upper limit for the AGNs of our sample considering a timescale for losses due to gravitational radiation equal to 1000 yr. The dashed vertical line marks $q = 1$.

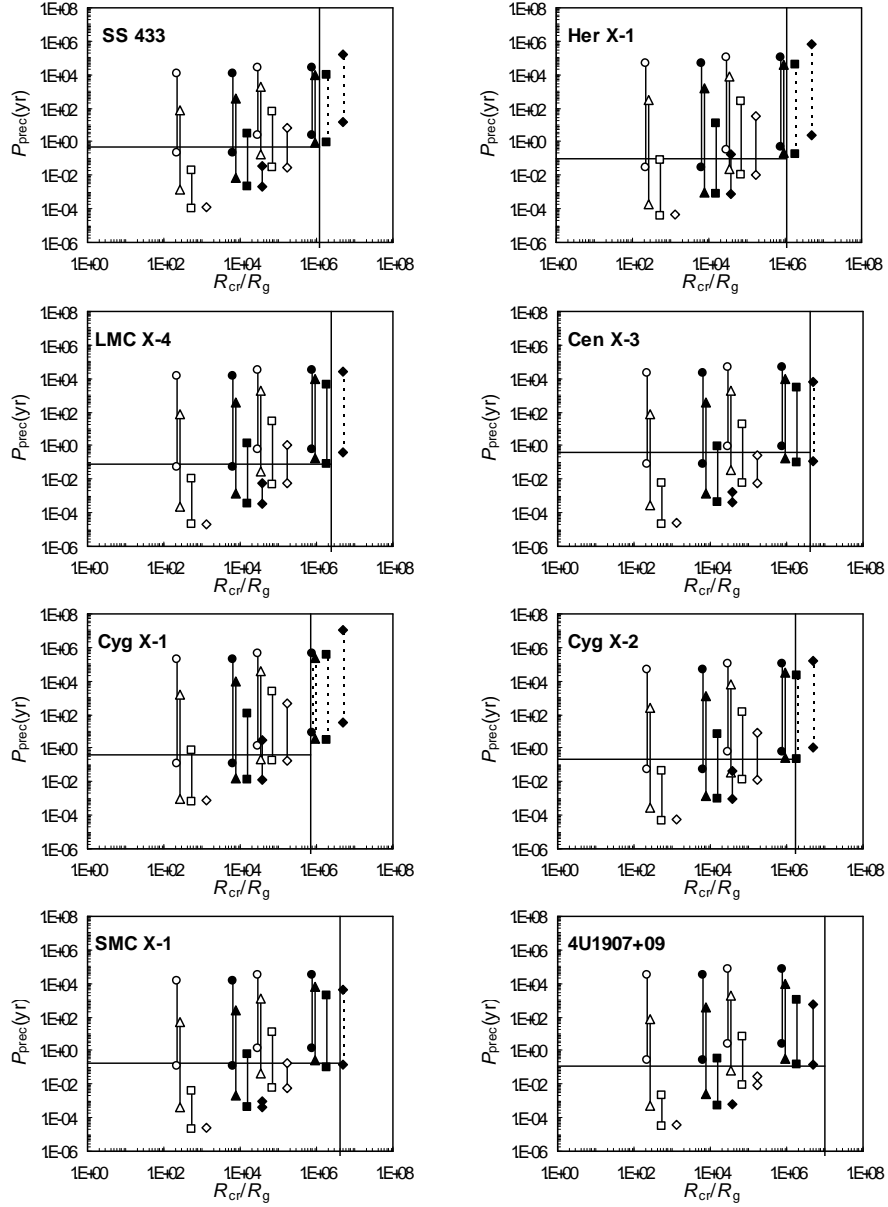


Fig. 2.— Precession due to the radiation torques in our sample of X-ray binaries. Circles, triangles, squares and diamonds correspond respectively to $s = -3/2, -1, 0$ and $3/2$. Filled symbols represent the case $\eta = f(\alpha)$ for $\alpha = 0.1$, while the open ones $\eta = 1$. The solid horizontal line in each panel refers to the observationally inferred precession period, while the vertical solid line mark the location of the outer disk radius. The allowed range for the precession period is represented by the connecting lines, whose extremes are given by the lower and upper limits of the surface density of the accretion disk at the gravitational radius. Model predictions beyond the outer disk radius (not physically acceptable) are plotted as dashed lines.

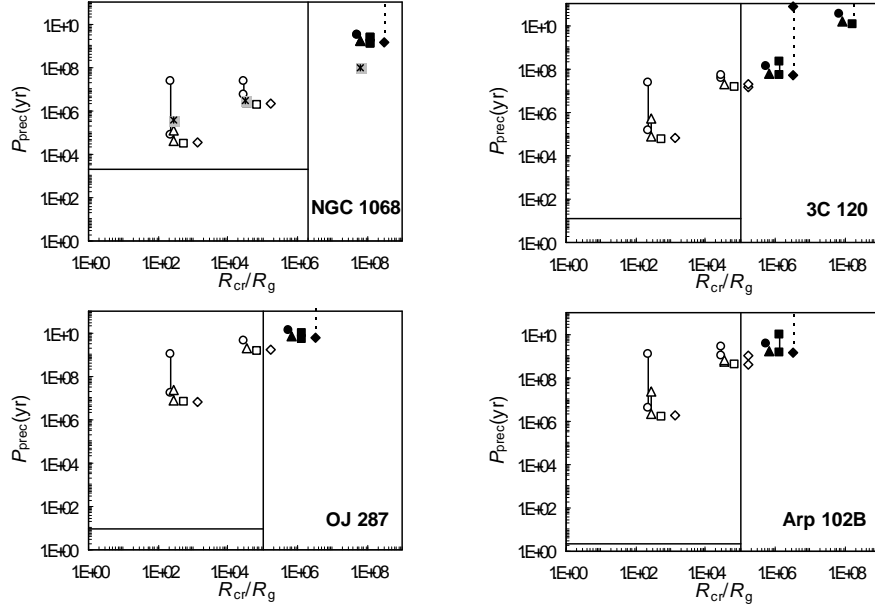


Fig. 3.— Precession due to the radiation torques applied to our sample of AGNs. Same nomenclature as in Figure 2 is assumed here. In the case of $\eta = f(\alpha)$, we have chosen $0.001 \leq \alpha \leq 0.012$ for NGC 1068 (Caproni, Abraham & Mosquera Cuesta 2006) and $\alpha = 0.01$ for the other sources. The crossed gray squares in the panel of NGC 1068 refer to the modeling of the accretion disk by Huré (2002) based on maser data. The solid horizontal line refers to the observationally inferred precession period. The vertical lines refer to the disks’ outer radii, 1.1 pc for NGC 1068 (inferred from interferometric maser observations Gallimore et al. 2004) and $10^5 R_g$ for the other sources (upper limit based on Collin-Souffrin & Dumont 1990).

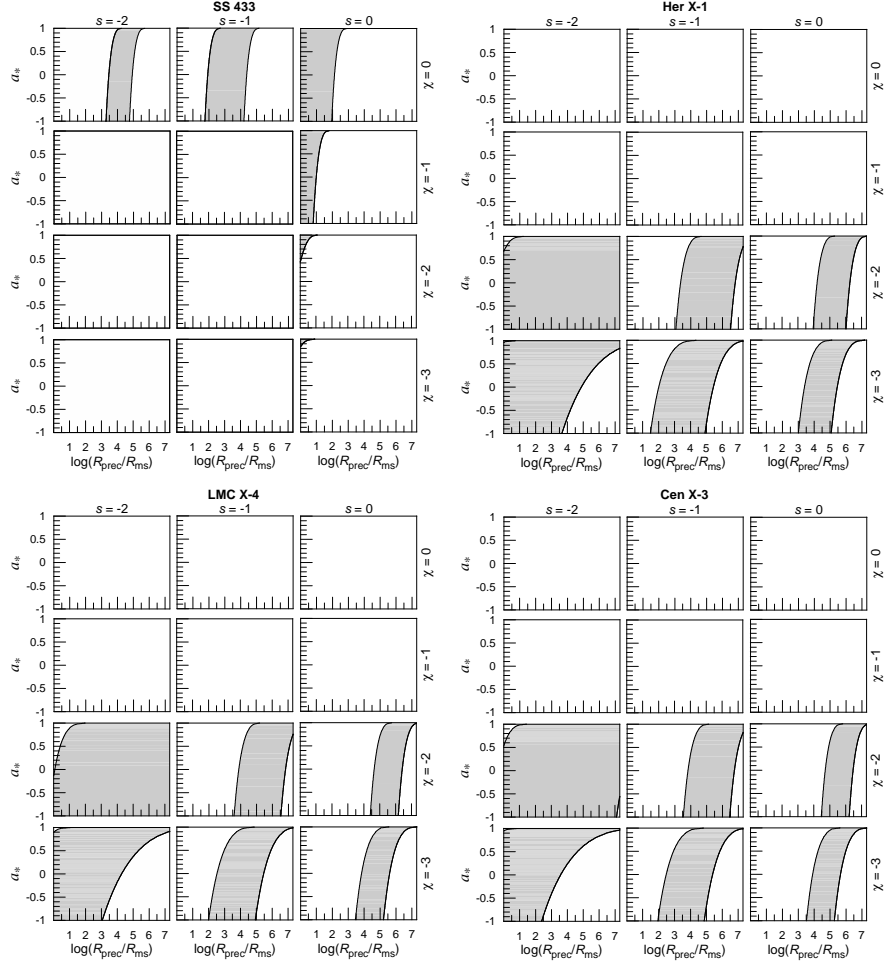


Fig. 4.— Magnetically-driven instability. The logarithm of $\tan \varphi P_{\text{prec}}^{\text{mag}} B_{0,Z}^2 / \Sigma_0$ is calculated as a function of the dimensionless spin parameter a_* and the outer radius of the warped/precessing part of the disk R_{prec} (normalized by the radius of the marginally stable orbit) for SS 433, Her X-1, LMC X-4 and Cen X-3. $P_{\text{prec}}^{\text{mag}}$ is given in years, while $B_{0,Z}$ and Σ_0 are in CGS units. The gray region in the panels correspond to the allowed range constrained by the observations considering $\tan \varphi = 1$. Calculations were performed (see text) for $s = -2, -1$ and 0 (from the left to the right side) and for $\chi = 0, -1, -2$ and -3 (from the top to the bottom panel).

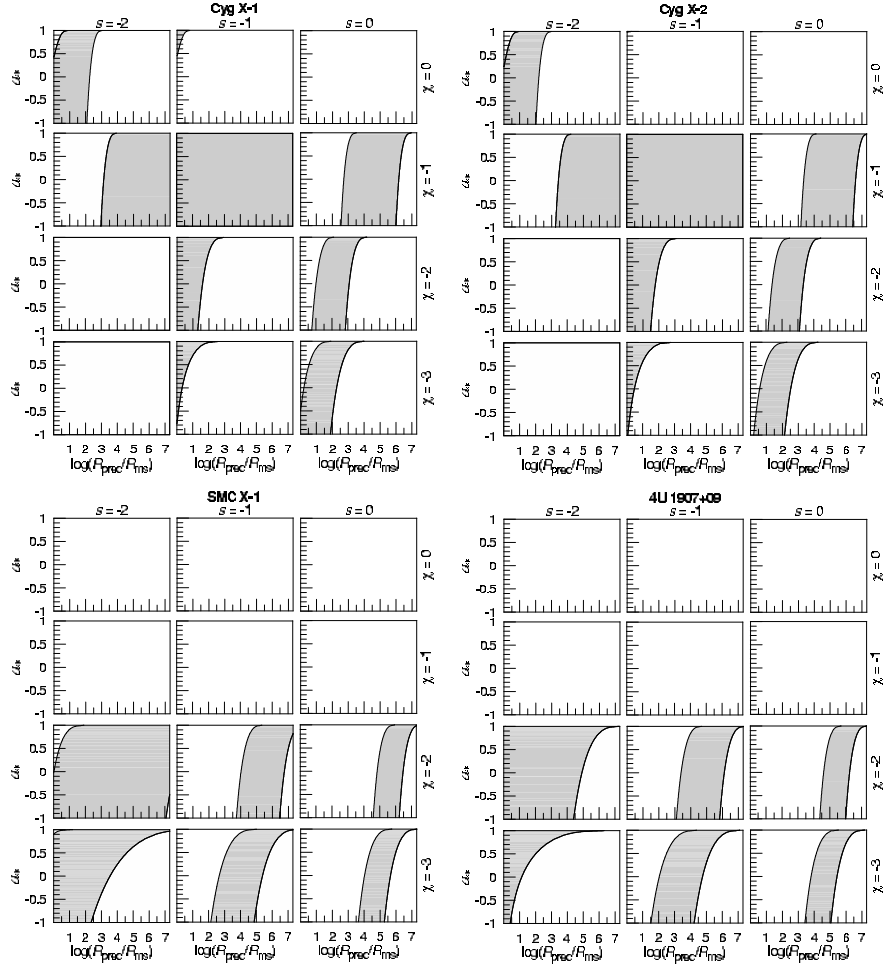


Fig. 5.— Magnetically-driven instability for the galactic sources Cyg X-1, Cyg X-2, SMC X-1 and 4U 1907+09. Same nomenclature as in Figure 4 is adopted here.

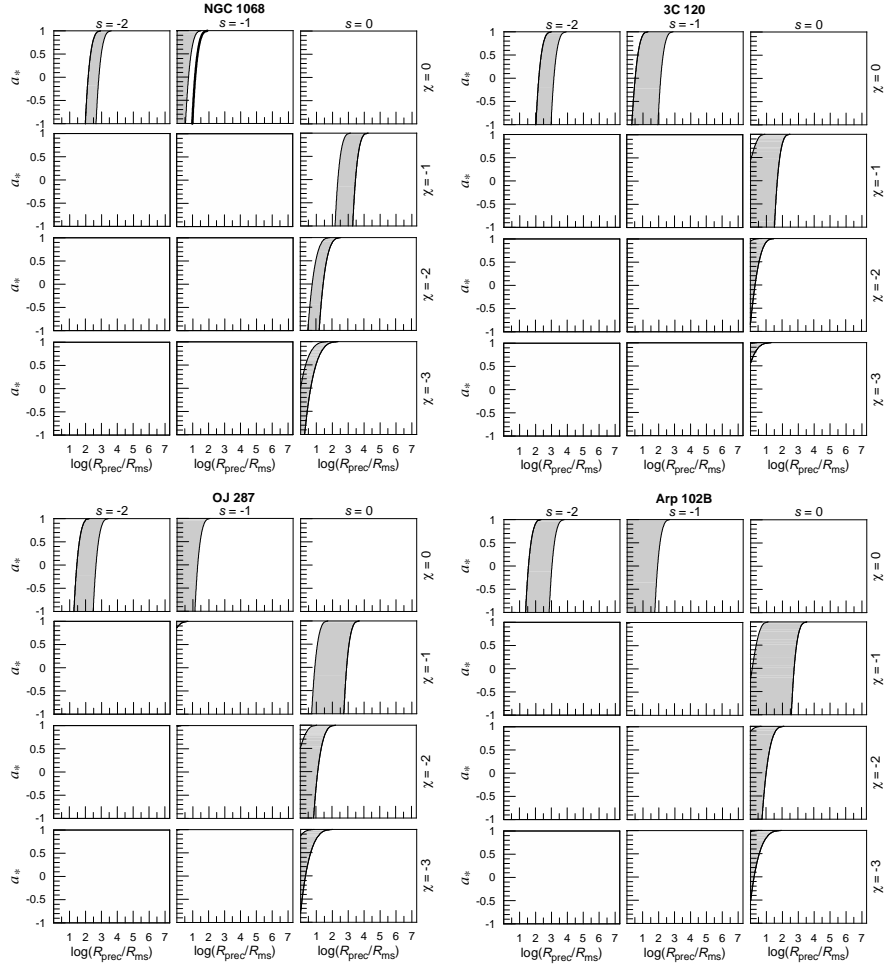


Fig. 6.— Magnetically-driven instability for the extragalactic sources NGC 1068, 3C 120, OJ 287 and Arp 102B. Same nomenclature as in Figure 4 is adopted here. The thick black line represents the solution for NGC 1068 found from the accretion disk model parameters given by Huré (2002) (see also Caproni, Abraham & Mosquera Cuesta 2006).

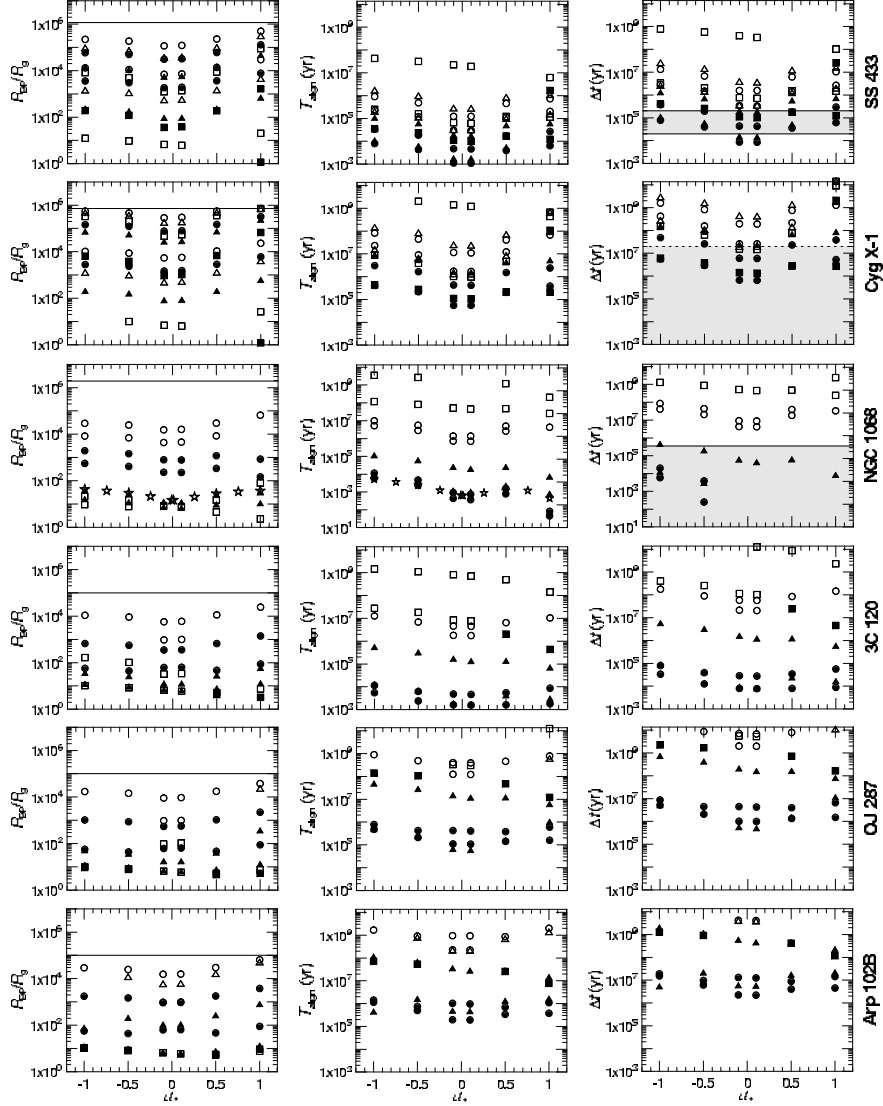


Fig. 7.— Bardeen-Petterson effect in accreting black holes. We show the Bardeen-Petterson radius, the timescale for the alignment between the angular momenta of the black hole and of the accretion disk, and the time interval for the system to reach the observationally inferred precession period. Circles, triangles and squares represent respectively the solutions for $s = -2, -1$ and 0 . Filled symbols correspond to $\eta = f(\alpha)$ ($\alpha = 0.1$, for SS 433 and Cyg X-1, and $\alpha = 0.01$ for the AGN sources) while the open ones are for $\eta = 1$. Stars in the panels of NGC 1068 show the results from the disk model parameters given by Huré (2002) (see also Caproni, Abraham & Mosquera Cuesta 2006). The horizontal lines in the panels on R_{BP} show the values of the disk outer radius. The two parallel lines in the Δt -plot for SS 433 are the estimated age of SS 433 (between 0.02 and 0.2 Myr; Zealey, Dopita, & Malin 1980), while the dashed line seen in the Δt -plot for Cyg X-1 is the approximated upper limit for the ages of HMXBs (van den Heuvel 1994). The upper limit for age of NGC 1068 is 3.5×10^5 yr (Wilson & Ulvestad 1987). All plots referring to timescales are truncated at 13.7 Gyr.

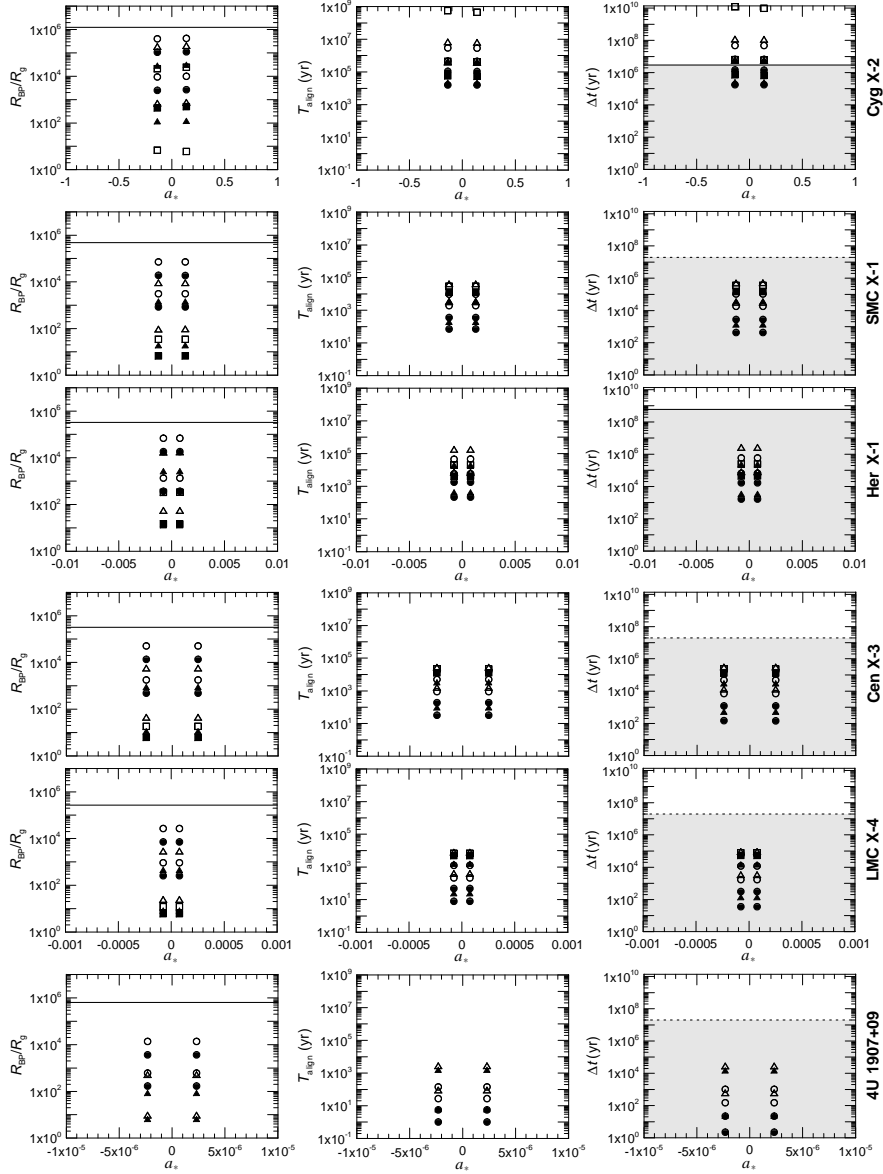


Fig. 8.— Bardeen-Petterson effect in accreting neutron star in X-ray binaries. Same nomenclature as in Figure 7 is adopted here. The lower limit for the age of Her X-1 is $\sim 6 \times 10^8$ yr (Verbunt, Wijers & Burm 1990), while the estimated age of Cyg X-2 is roughly 3 Myr (Kolb et al. 2000).